

Biogeochemical impact of summertime coastal upwelling on the New Jersey Shelf

Scott Glenn,¹ Robert Arnone,² Trisha Bergmann,¹ W. Paul Bissett,³ Michael Crowley,¹ Jay Cullen,⁴ Joe Gryzmski,⁵ Dale Haidvogel,¹ Josh Kohut,¹ Mark Moline,⁶ Mathew Oliver,¹ Cris Orrico,⁶ Robert Sherrell,¹ Tony Song,⁷ Alan Weidemann,² Robert Chant,¹ and Oscar Schofield¹

Received 23 December 2003; revised 22 June 2004; accepted 22 July 2004; published 24 December 2004.

[1] The alternative hypothesis that observed regions of recurrent hypoxia on the New Jersey inner shelf are more related to coastal upwelling than riverine inputs of nutrients was investigated through a series of multidisciplinary research programs beginning in 1993. The largest variations in ocean temperatures along the New Jersey coast, other than seasonal, are found to be caused by episodic summertime upwelling events driven by southwesterly winds associated with the atmospheric Bermuda High. Off the southern coast of New Jersey, topographic variations associated with ancient river deltas cause upwelled water to evolve into an alongshore line of recurrent upwelling centers that are colocated with historical regions of low dissolved oxygen. Recurrent upwelling centers are observed every summer in a 9-year data set. The most significant upwelling events occur in summers following colder than usual falls and winters. Size and duration of individual events are correlated and are found to depend on the wind forcing history that effects the inner side of the Middle Atlantic Cold Pool, the precipitation history that effects the strength of the Hudson River plume, and the mixing storm frequency. Upwelling results in a significant enhancement of particulate organic carbon. The typical carbon enhancement associated with the upwelling is sufficient to deplete 75% of the oxygen in the bottom water, making it borderline hypoxic. This indicates that topographically controlled coastal upwelling, rather than riverine inputs, is the more probable mechanism for generating the historical regions of recurrent hypoxia observed along the New Jersey coast. **INDEX TERMS:** 4279 Oceanography: General: Upwelling and convergences; 4552 Oceanography: Physical: Ocean optics; 4219 Oceanography: General: Continental shelf processes; 4805 Oceanography: Biological and Chemical: Biogeochemical cycles (1615); **KEYWORDS:** coastal upwelling, phytoplankton, hypoxia

Citation: Glenn, S., et al. (2004), Biogeochemical impact of summertime coastal upwelling on the New Jersey Shelf, *J. Geophys. Res.*, 109, C12S02, doi:10.1029/2003JC002265.

1. Introduction

[2] A widespread decline in bottom dissolved oxygen (DO) levels to hypoxic/anoxic conditions impacted nearly

the entire New Jersey continental shelf in 1976, resulting in over \$550 million in losses to the shellfishing and related industries [Figley *et al.*, 1979]. Falkowski *et al.* [1980] identified a causal series of events that included large runoff during a warm winter resulting in early stratification of the shelf, continued development of a strong deep summer thermocline during an unusually hot summer, persistent southerly winds with fewer than usual storms, a large subsurface phytoplankton bloom with low grazing by zooplankton, and respiration and decomposition of the bloom below the seasonal thermocline. This massive extreme event [Atwood *et al.*, 1979] prompted the initiation of several long-term DO monitoring programs that established statistics on the more typical annual occurrences of hypoxia along the New Jersey coast. Stoddard *et al.* [1986] documented hypoxic conditions in over one third of the summertime bottom water observations from 1977–1985, finding reduced bottom DO levels concentrated inshore of the 20-m isobath. They suggested that the reduction was

¹Coastal Ocean Observation Lab, Institute of Marine and Coastal Sciences, Rutgers University, New Brunswick, New Jersey, USA.

²Ocean Color Section, Naval Research Laboratory, Stennis Space Center, Mississippi, USA.

³Florida Environmental Research Institute, Tampa, Florida, USA.

⁴School of Earth and Ocean Sciences, University of Victoria, Victoria, British Columbia, Canada.

⁵Division of Earth and Ecosystems Science, Desert Research Institute, Reno, Nevada, USA.

⁶Biological Sciences Department, California Polytechnic State University, San Luis Obispo, California, USA.

⁷Jet Propulsion Laboratory, California Institute of Technology, Pasadena, California, USA.

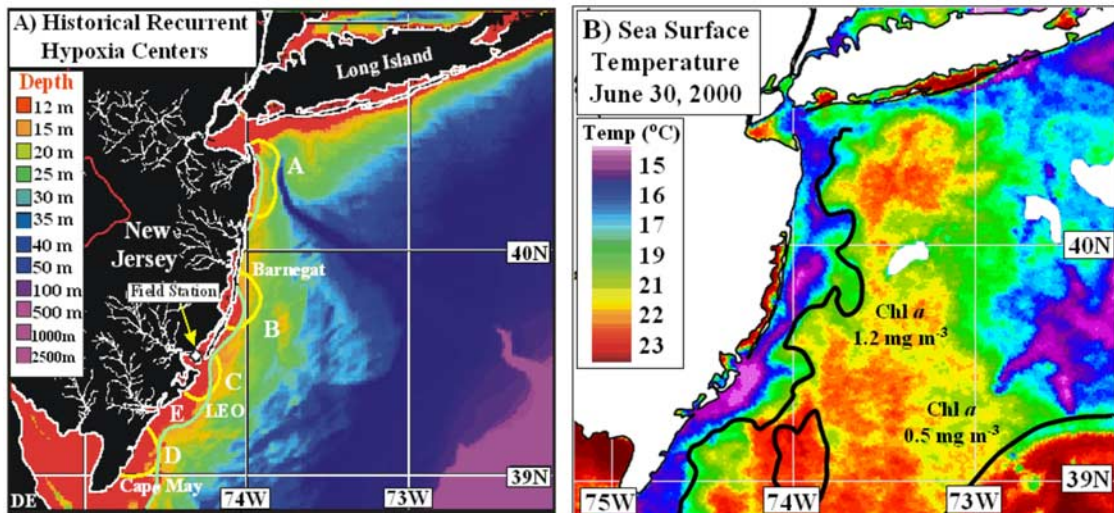


Figure 1. (a) Bathymetry map for the New Jersey continental shelf where the four regions (yellow arcs) of recurrent hypoxia [Warsh, 1987] are highlighted. The 13-m isobath is highlighted in green. Note the peaks of this isobath's offshore extent are offset just to the south of the hypoxic areas. Rivers and streams defining coastal watersheds are shown. (b) AVHRR SST image showing multiple upwelling centers along the New Jersey Coast. Two contours showing chlorophyll *a* values derived from a SeaWiFS image on the same day are superimposed on the SST. The peak chlorophyll values correlate with the low-temperature water in the SST image.

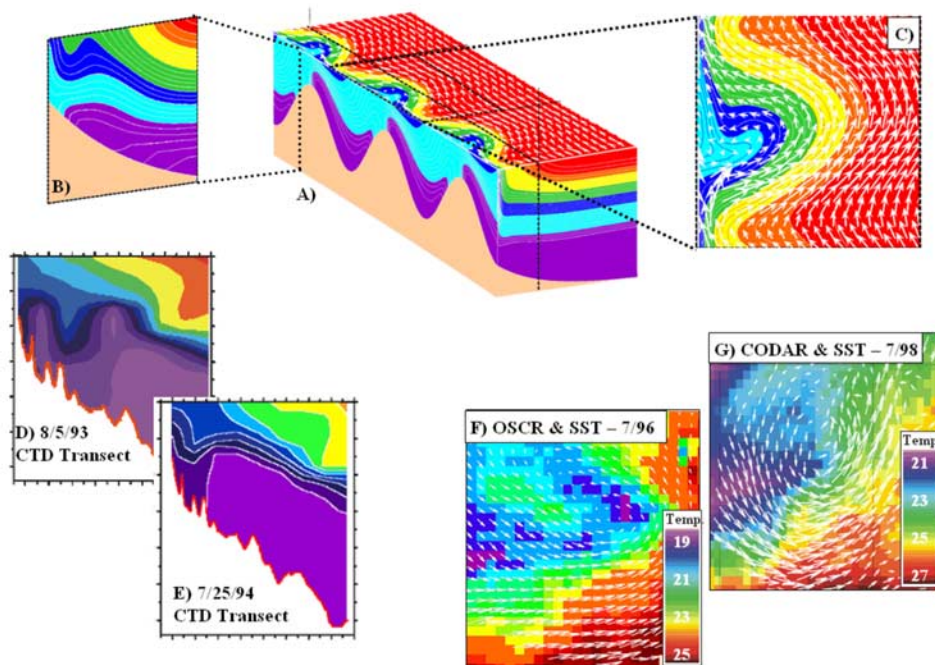


Figure 2. Idealized modeled upwelling over topographic highs/deltas similar to the New Jersey coastline. (a) A 3-D view highlighting the Barnegat, LEO, and Cape May deltas (shown in Figure 1a). Upwelling centers are formed on the downstream side of each topographic high. (b) Vertical cross section on the downstream side of the topographic high showing the development of an offshore cold dome. (c) Enlargement of the surface current and temperature field for one of the upwelling eddies. (d) and (e) Vertical CTD transects through an upwelling center illustrating the development of the cold dome within the Mullica River Estuary upwelling center. (f) and (g) HF radar-derived surface current fields and satellite-derived SSTs illustrating the development of an upwelling eddy offshore the Mullica River Estuary.

caused by a series of events starting with phytoplankton blooms in the euphotic zone above the pycnocline, where the uptake of nutrients by phytoplankton produces oxygen and organic matter. The organic matter produced eventually accumulates below the pycnocline, and as it decays, depletes the oxygen and increases ammonium, which is further oxidized to nitrate. *Swanson and Parker* [1988] further noted that the bottom hypoxic conditions in a decade of DO observations off New Jersey were strongly correlated with deep pycnoclines and strong persistent southerly to southwesterly winds.

[3] *Steimle* [1978] and *Warsh* [1987] found that hypoxic conditions were often clustered offshore specific estuaries and inlets. These regions of recurrent hypoxia identified on their charts were located offshore the (A) Hudson-Raritan estuary, (B) Barnegat Inlet, (C) the Mullica River estuary, and (D) Townsend/Hereford Inlets (Figure 1a). The observed spatial distribution led to the initial hypothesis found in these reports that the nutrient source for the phytoplankton blooms may be terrestrial. This, however, raises the question of why specific estuaries with very different characteristics are associated with recurrent hypoxia, while some estuaries with very similar characteristics are not. The Hudson and Raritan Rivers are among the earliest industrialized rivers in the nation and are heavily impacted by anthropogenic sources of nutrients. In contrast, nearly the entire Mullica River watershed is within the protected Pinelands National Reserve, yet it is still associated with a region of recurrent hypoxia. Barnegat Inlet is the entrance to the 60-km-long Barnegat Bay, which is heavily populated and also receives inputs from major rivers. In contrast to this, Townsend and Hereford Inlets are entrances to small 2–3-km-wide bays with no major river inputs. Additionally, the watershed for the Great Egg Harbor River also is partially contained within the Pinelands National Reserve and thus is very similar to the Mullica watershed. However, no region of recurrent hypoxia is observed offshore of the (E) Great Egg Harbor River estuary.

[4] The apparent inconsistencies with riverine inputs as the dominant source of nutrients, and the observed correlation with southerly winds, led us to begin (in 1993) investigations of the alternative hypothesis that the nutrient source for the phytoplankton blooms that eventually lead to the recurrent hypoxia regions are more related to coastal upwelling. However, early studies (pre-1990s) of coastal upwelling on the New Jersey shelf are few. *Beardsley and Boicourt* [1981] report that the long-term mean flow in the Mid-Atlantic Bight (MAB) is slow (order 5 cm/s) and generally southward, but that the actual flow on any given day is much more likely to be a more energetic response in either alongshore direction driven by episodic wind events. Only *Hicks and Miller* [1980] report a strong correlation between southerly winds and rapid decreases in surf zone temperatures of up to 8°–9°C over 2–3 days. They attribute the large and rapid changes to wind forcing of a strong summer thermocline and the MAB Cold Pool. The Cold Pool is historically defined as the 8°C or less bottom water that remains over the summer, shoreward of the shelfbreak between Georges Bank and the Virginia Capes [*Houghton et al.*, 1982]. The shoreward edge of the Cold Pool is quite variable. *Hicks and Miller* [1980] report observations of

9°C bottom water within 1 km of the shore during a sustained southerly wind event in July 1973; yet in July 1974, they found the 9°C isotherm surrounding the Cold Pool remained 75 km offshore. Even though coastal upwelling may be a source of nutrients, *Stoddard et al.* [1986] point out that it also is a potential source of oxygen, since the colder waters offshore also contain the highest concentrations of DO. Thus the actual mechanism of nutrient supply, where in the water column the phytoplankton blooms occur (above or below the thermocline), and the processes and timing of the events leading to hypoxia on the New Jersey shelf were virtually undocumented in the pre-1990s literature.

[5] The approach to investigate the hypothesis that recurrent hypoxia was more related to coastal upwelling rather than riverine inputs was to select one of the regions of recurrent hypoxia and focus on its detailed evolution over a series of summers. The (C) Mullica River Estuary was chosen because of its central location between the other two southern New Jersey regions, and its convenient proximity to the existing Rutgers University Marine Field Station (RUMFS) and the envisioned Long-Term Ecosystem Observatory (LEO) [*Grassle et al.*, 1998] (Figure 1). Field studies began in 1993 and continued each summer until 2001. Coordinated modeling studies provided guidance to the sampling programs throughout, with idealized model results [*Glenn et al.*, 1996] available early in the program, and real-time data assimilative model forecasts for adaptive sampling available during a series of Coastal Predictive Skill Experiments (CPSEs) focused on coastal upwelling [*Glenn et al.*, 1998; *Schofield et al.*, 2002, 2003] during the later years. This paper summarizes the results of these field studies as they relate to coastal upwelling, the resulting phytoplankton blooms, and the potential for those blooms to deplete bottom dissolved oxygen concentrations. Our analysis methods are described first, followed by a summary of the physical setting, and concluding with a summary of the biogeochemical impacts as they relate to hypoxia.

2. Methods

2.1. Meteorology and Remote Sensing

[6] Local weather observations were collected at the RUMFS meteorological tower outfitted with a suite of Improved Meteorological (IMET) sensors. Wind speed and direction, air pressure, temperature and humidity, and incoming solar radiation are sampled every second and archived as 1-min averages over the duration of this study. Direct broadcast advanced very high resolution radiometer (AVHRR) data were collected from the constellation of NOAA Polar Orbiting Environmental Satellites using an SeaSpace L Band data acquisition system and converted to sea surface temperature (SST) using standard algorithms [*Bernstein*, 1982; *McClain et al.*, 1985]. Clouds were removed and the images hand navigated by the methods described by *Glenn and Crowley* [1997]. In the summary statistics that follow, morning AVHRR passes were used to avoid the effects of solar heating. Coincident with the beginning with the

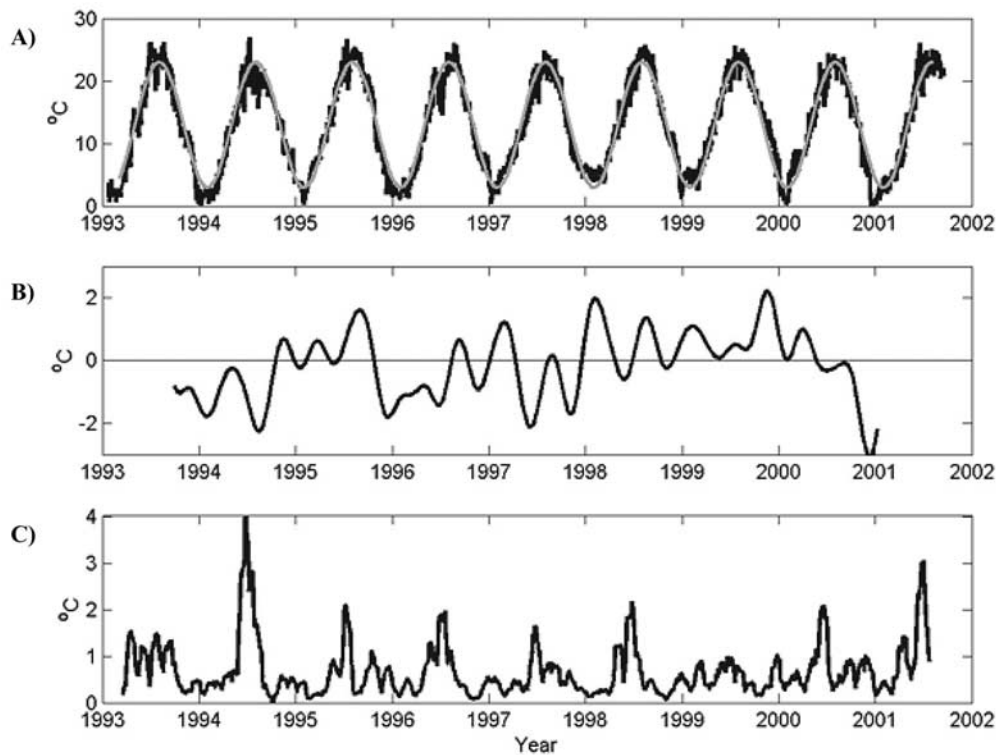


Figure 3. (a) Satellite-derived SST measured over the 9-year effort at the LEO research site (6 km offshore). Black is the data, and grey is the fit of a seasonal cycle. (b) The 30-day low-pass-filtered temperature anomalies from the seasonal cycle. (c) RMS difference between the raw temperatures and a 3-day running mean.

CPSEs in 1998, daily ocean color imagery was locally acquired from the SeaWiFS satellite. SeaWiFS data were processed using the NASA Data Archive and Analysis Center (DAAC) algorithms. Surface current data were collected by an Ocean Surface Current Radar (OSCR) system operated by the University of Miami in 1996, and by the Rutgers CODAR network [Kohut *et al.*, 1999] beginning in 1998. OSCR data processing is described by Chant [2001], and CODAR data processing is described by Kohut and Glenn [2003].

2.2. Cabled Observatory

[7] A 10-km-long electro-optic cable, installed in 1996, connects the RUMFS to a retrievable pair of instrumented subsea nodes located 1.5 km apart on the New Jersey inner shelf [Grassle *et al.*, 1998]. The subsea nodes typically are outfitted with a fixed pressure sensor, and a manually controlled vertical profiler equipped with, at minimum, a conductivity-temperature-depth (CTD) sensor. During the latter years of this study, a bio-optical profiling package outfitted with a Wetlabs absorption attenuation meter (ac-9), a HOBI lab Hydrosat-2, and Sequoia Laser in Situ Scatterometer and Transmissometer (LISST) system was deployed during the upwelling season [see Oliver *et al.*, 2004].

2.3. Ship Sampling

[8] In situ data were collected by multiple research vessels to spatially expand the cabled observatory time series. The research vessels were of two different categories.

One category of vessels conducted rapid high-resolution surveys, providing real-time data to the rest of the research fleet. These vessels were equipped with towed systems to provide rapid vertical sections of data beneath the surface remote sensing data. Typically the instrumentation includes a surface-towed downward facing acoustic Doppler current profiler (ADCP) and a Guildline Inc. undulating MiniBat equipped with CTD/Fluorometer/Optical Backscatter sensor package. Data from this vessel were transferred, via Freewave radio modem, back to shore in real-time to guide other ships to adjust sampling transects “on the fly”. Analysis of the towed data is described by Chant *et al.* [2004]. The second category of research vessel is outfitted with profiling instruments. Specific transect lines and the locations of the stations were determined by the real-time data from the ships and satellites [Schofield *et al.*, 2002]. At each station, vertical profiles of optical and physical data were collected using an integrated bio-optical package. The bio-optical package consisted of a Wetlabs absorption/attenuation meter (ac-9), a Falmouth CTD, a profiling Saatlantic spectral radiometer, a Sequoia LISST, and a HOBI Labs Hydrosat-6 backscatter sensor. The measurements of the inherent optical properties used in this study were collected using the standard nine wavelengths of the Wetlabs ac-9. At each station, the instrument was lowered to depth to remove air bubbles and the instrument was allowed to equilibrate to ambient temperature before the data were collected. Only data from the upcasts were utilized. Data were averaged into 0.25-m depth bins for all subsequent analyses. The instruments

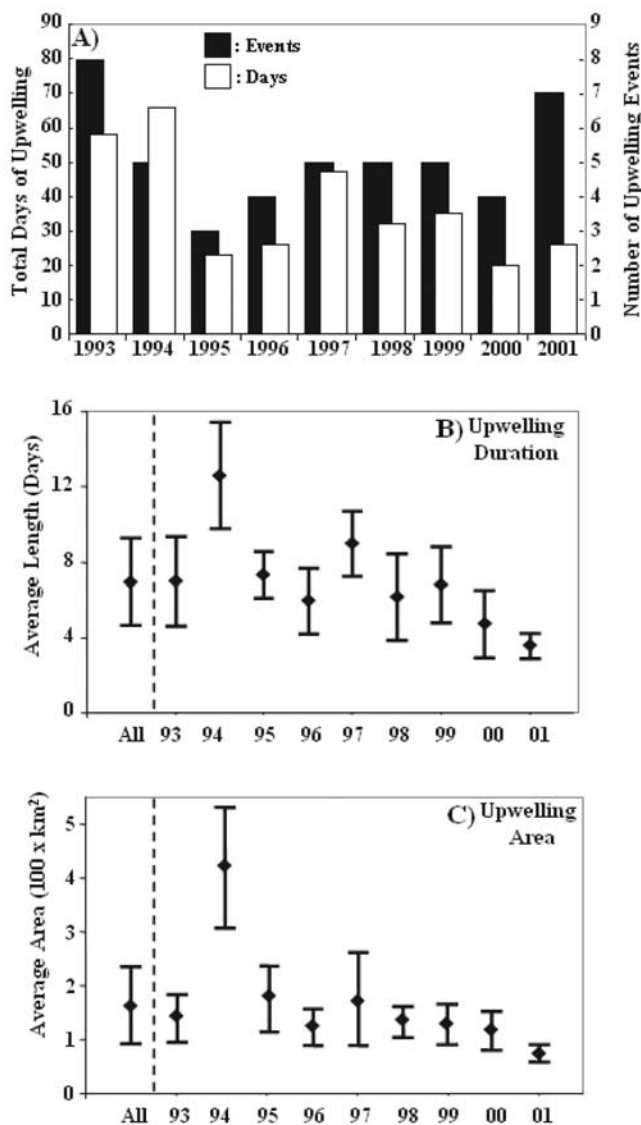


Figure 4. (a) Total number of upwelling days and number of upwelling events observed each summer for the Mullica River Estuary upwelling center. Upwelling was defined as a 2°C temperature difference between the colder upwelled water and the warm water offshore. (b) Average and standard deviation of the duration of upwelling events for the Mullica River Estuary upwelling center. (c) Average and standard deviation of the maximum area for each upwelling event for the Mullica River Estuary upwelling center.

were factory calibrated prior to the field season. Manufacturer recommended protocols (<http://www.wetlabs.com/otherinfo/ugftp.htm>) were used to track instrument calibration throughout the field season. This included clean water, temperature, and salinity calibrations.

2.4. Discrete Water Measurements

[9] At each station, water was collected with Niskin bottles from both surface and bottom waters. Aliquots were filtered, under low vacuum (<10 cm Hg), through GF/F (Whatman) glass fiber filters to concentrate the particles for

pigment and absorption determinations. Filters were placed into snap top vials and quick frozen in liquid nitrogen. Samples were stored at -80°C until later analysis.

2.5. Particulate Trace Metals

[10] Utmost care was taken to avoid contamination during sampling and subsequent handling and analysis of samples [Cullen *et al.*, 2001]. After Suspended Particulate Matter (SPM, corrected for NaCl content) determinations, filter digests were analyzed for Al and Fe as well as nine other trace elements by magnetic sector high-resolution inductively coupled plasma mass spectrometer (HR-ICP-MS). Overall analytical precision was $\pm 6\%$ for Al and $\pm 2\%$ for Fe based on five replicate analyses of a single sample digest. Blank solutions (10% HNO_3) were analyzed periodically throughout the run to verify maintenance of low ($<5\%$ of lowest sample analyzed) and constant blank for both Al and Fe. The contribution of Al and Fe blank from digest vials and acids was minimal ($<0.6\%$ and $<0.1\%$ of lowest sample).

2.6. POC and PON Measurements

[11] Filters were analyzed for organic carbon and nitrogen content using a Carlo-Erba model NA 1500 series 2 CHN analyzer. The precision of the method was $\pm 1.5\%$ (2σ) for C and $\pm 4.8\%$ (2σ) for N based on replicate analysis of acetanilide standard.

2.7. Dissolved Oxygen

[12] Dissolved oxygen was measured using high-precision Winkler titrations according to Friederich *et al.* [1991]. Samples were collected and preserved at sea for later analysis. The dissolved oxygen was collected during a 3-year monthly time series of cross-shore transects [Boehme *et al.*, 1998].

2.8. Phytoplankton Pigmentation and Absorption

[13] Aliquots of all whole water samples were analyzed for the lipid-soluble algal pigments using reverse phase HPLC procedures [Wright *et al.*, 1991]. The contribution of the different algal taxa to total chlorophyll was calculated using CHEMTAX as described by Millie *et al.* [2001]. Whole cell absorption spectra and methanolic extractions were measured using the filter pad technique and Kishino extractions [Cleveland and Weidemann, 1993; Kishino *et al.*, 1985].

3. Results and Discussion

3.1. Physical Setting

[14] Historical atmospheric observations for the Middle Atlantic Bight indicate that the wind over the shelf is mostly from the northwest over most of the year, and mostly from the southwest during the summer [Moore *et al.*, 1976]. The variability is dominated by weather events with a spectral peak near three days [Saunders, 1977]. Kohut *et al.* [2004] examined data from the RUMFS meteorological tower and found that the distribution of hourly average winds during the summer stratified season was bimodal, with alongshore winds dominating both from the southwest (upwelling favorable) and from the northeast (downwelling favorable). Persistent southwesterly winds are often associated with the atmospheric Bermuda high-pressure system and thus often

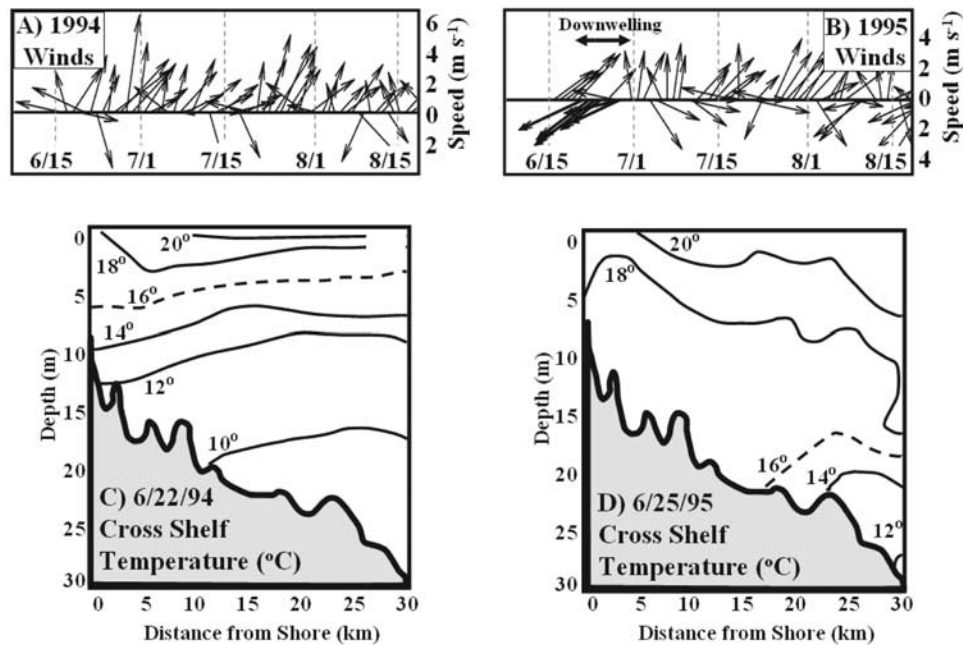


Figure 5. A comparison of the summer winds and hydrography for (a) and (c) 1994 and (b) and (d) 1995. Both summers tended toward upwelling favorable winds. The 16°C isotherm is (c) inshore in 1994 and (d) offshore in 1995 after a week of strong downwelling favorable winds were experienced (Figure 5b).

would persist for several days to a week, longer than the typical alongshore winds from the northeast often associated with offshore storms.

[15] Atmospherically forced cross-shelf transport has a significant effect on inner shelf temperature and phytoplankton distributions along the New Jersey coast, and are readily detectable by satellite [Glenn *et al.*, 1996]. Upwelling events observed in the satellite-derived SSTs often begin as a very narrow band of cold water along the coast that initially may be only a few kilometers wide. If southwesterly winds persist, the band of cold water progressively widens in the offshore direction. Within a matter of days, wave-like structures develop on the offshore front between the cold upwelled water and the warm surface layer water, especially after relaxations in the upwelling favorable winds. Figure 1b illustrates a typical upwelling event in a satellite-derived SST and chlorophyll *a* map. SST fronts and chlorophyll fronts are clearly correlated. A well-developed upwelling center is observed offshore the Mullica River estuary. Within the distinct upwelling centers that develop, the coldest upwelled water often is found in the middle of the offshore extensions of the waves, not at the coast. The SST image also reveals a commonly observed asymmetry in the upwelling center, with a narrower upstream side on the south, and a cold frontal filament extending offshore to the northwest on the wider northern side. The figure further illustrates that on the shelf-wide scale, SSTs generally increase and chlorophyll *a* concentrations generally decrease in the offshore direction.

[16] The trend observed by Glenn *et al.* [1996] for the upwelling centers to form in the same locations persisted year after year throughout the 9-year SST data set. Along the southern New Jersey coast, recurrent upwelling centers were observed offshore of Barnegat Inlet, the Mullica River

Estuary, and Townsend/Hereford Inlets. These three recurrent upwelling centers are thus collocated with the three recurrent hypoxia regions along the southern New Jersey coast. When compared to the topography in Figure 1a, the recurrent centers are located just downstream of a series of topographic highs associated with ancient river deltas. Numerical studies of coastal upwelling demonstrated that the idealized alongshore variation in bottom topography can explain the formation of these recurrent upwelling centers [Glenn *et al.*, 1996; Song *et al.*, 2001]. Initialized with typical midsummer density profiles, and forced by a constant southerly wind stress (1 dyn/cm²), within 3 days the idealized model (Figures 2a–2c) developed a surface velocity field (top of Figure 2a) consisting of a broad coastal jet meandering northward around a cyclonic eddy that forms downstream of each topographic high. An enlargement of the eddy surface structure (Figure 2c) details the downwind current on the warm side of the upwelling front that wraps around an asymmetrical eddy that is beginning to form a filament-like structure extending offshore to the northwest. At the coast, an upwind countercurrent is generated. The vertical cross section on the upstream side of the topographic high (side of Figure 2a) reveals a subsurface temperature structure that monotonically decreases as one approaches the shore and the bottom. The vertical cross section (Figure 2b) on the downstream side of the topographic high passes through the eddy to reveal the development of an offshore cold dome in the upwelled isotherms. These raised isotherms are associated with the offshore and northwestward advection of cold water by the cyclonic eddy. The depressed isotherms in the middle of the upwelling are associated with the onshore and southward advection of warm water by the eddy. This three-dimensional (3-D) advective process is fundamentally different from the inner

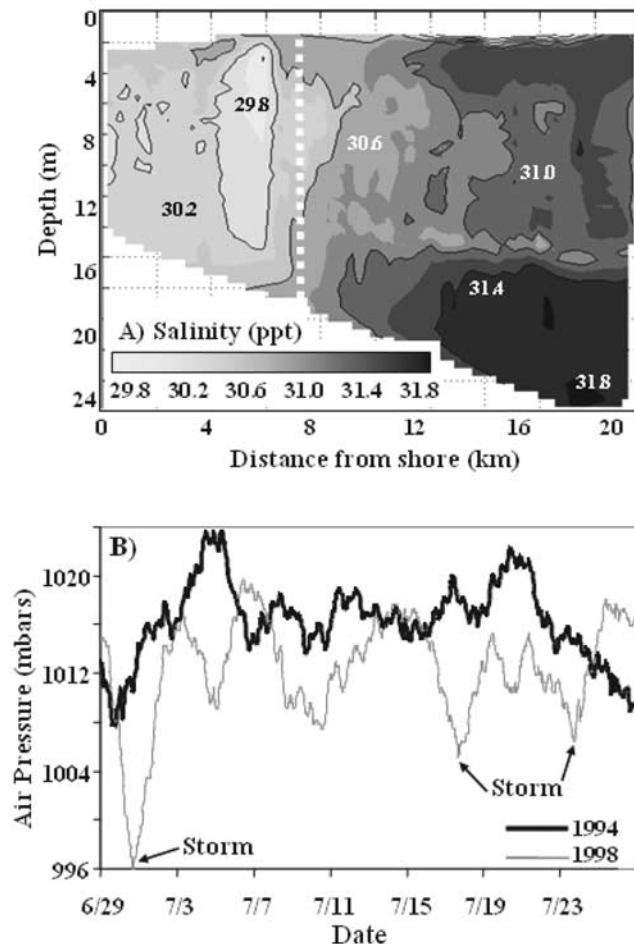


Figure 6. (a) A low-salinity plume encountered in nearshore waters in the summer of July 2000 because of heavy precipitation and coastal runoff. The large volume of water implies the source was most likely the Hudson River. (b) The storm frequency in the summers of 1994 and 1998 are compared. During 1994, the year of greatest upwelling intensity, there were few low-pressure systems that disrupted upwelling events. In 1998 there was a series of low-pressure storms that effectively mixed nearshore waters for most of the month of July.

shelf mixing process *Austin and Lentz* [2002] identified as causing the upwelling cold dome in their 2-D model simulations that included the Mellor-Yamada closure scheme. Early observational studies of the upwelling eddies focused on the identification of this offshore cold dome in CTD transects, two examples of which are displayed Figure 2d. They both reveal an offshore cold dome, consistent with the advective processes identified in the *Glenn et al.* [1996] model runs. The 1993 section also begins in water sufficiently shallow to reveal a more well mixed region nearshore, forming a second inner shelf cold dome consistent with the *Austin and Lentz* [2002] mechanism. Later the addition of high-frequency (HF) radar to the observational network enabled the upwelling eddy surface currents to be mapped. Two examples of the HF radar-derived surface currents showing the upwelling eddy overlaid on satellite SST maps are shown in Figure 2e. The downwind jet on the offshore side, and

the nearshore countercurrent, are observed with both radar systems. The idealized model simulations also suggest that the topographic variations do not change the absolute amount of upwelling, but instead redistribute upwelled water unevenly along the coast [*Song et al.*, 2001]. Thus at specific locations upwelling intensity, and its resulting biogeochemical impacts, are enhanced.

[17] The time variation of the upwelling is next characterized using a point near the middle of the Mullica River Estuary upwelling center, which in this case also corresponds to the location of LEO. Figure 3a illustrates the 9-year SST record for the LEO site assembled from the AVHRR satellite sensors. Seasonal variations obviously dominate the signal, with rapid and nearly linear transitions between the more stable winter and summer conditions. A fit of a seasonal cycle to the temperature record has an amplitude of 21°C with the warmest day during July, the coldest day in January. One seasonal anomaly readily observed in the time series itself is the warmer than average El Niño winter of 1998. To further quantify seasonal anomalies for the entire record, the daily temperature anomaly from the seasonal cycle was low-pass filtered with a 30-day window and plotted in Figure 3b. Cooling seasons (fall–winter) for 1993–1994, 1995–1996, and 2000–2001 are the most severe. In contrast, the mildest cooling seasons occur back-to-back in 1998–1999 and 1999–2000. High-frequency variability in the 9-year temperature record was then examined by calculating the RMS difference between the raw temperature data and a 3-day running mean (chosen to be consistent with the 3-day spectral peak in wind forcing). Peaks associated with coastal upwelling (Figure 3c) between 1° and 4°C are common in the summer periods at this inner shelf location. At several locations as close as 20 km farther offshore from LEO, similarly calculated high-frequency temperature changes rarely exceed 1°C , with the most notable short-term temperature changes being storm induced mixing in the fall. Thus the greatest high-frequency variations in temperature occur nearshore within the upwelling center. The magnitude of the upwelling-induced high-frequency variability (Figure 3c)

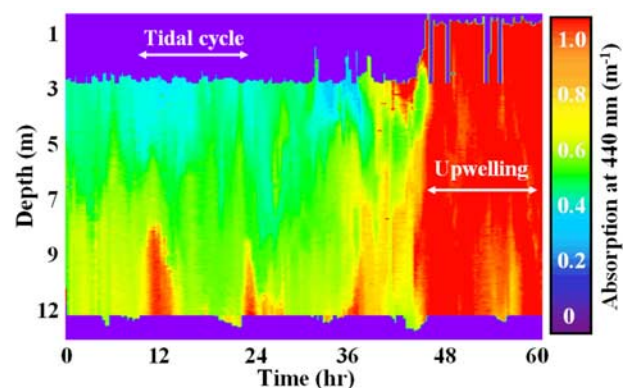


Figure 7. A 60-hour time series of total absorption (m^{-1}) at 440 nm collected during the initiation of an upwelling event in the summer of 1999. The data were collected via an electro-fiber-optic cable running a vertically profiling optical package [*Schofield et al.*, 2002]. The upwelling, which began at about hour 47, was associated with an immediate increase in the absorption.

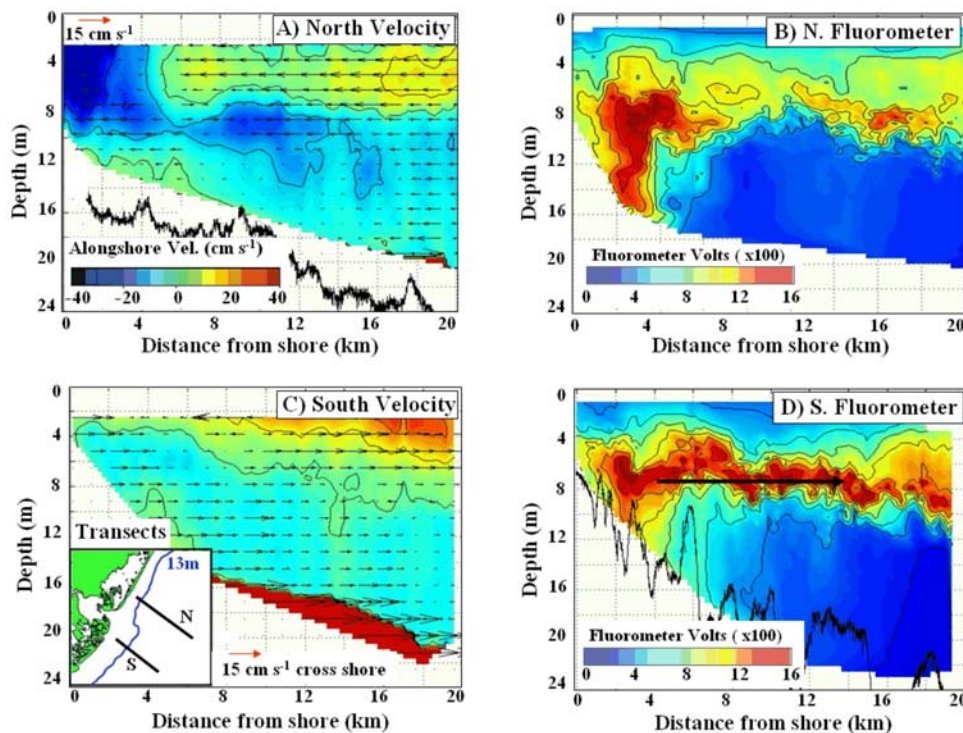


Figure 8. Cross-shelf transects from 12 July 2001 where data were collected using an undulating Guildline CTD/Fluorometer system and a surface-towed ADCP. Alongshore velocity is contoured, and cross-shore velocity is plotted as arrows. (a) The ADCP velocity cross-shelf section taken north of the upwelling eddy (see the inset map in Figure 8c), which is delineated by a southward flowing jet of water (blue is flow to the south) in the nearshore waters. (b) The fluorometry cross section with enhanced chlorophyll values associated with the southward flowing jet. (c) A cross section of current on the southern edge of the upwelling indicating that the alongshore jet is no longer present and there is enhanced transport offshore (delineated by the arrows). (d) The fluorometry cross section associated with the currents in Figure 8c. Enhanced material concentrations are flowing offshore with most material within the thermocline, which is below the detection limits of passive ocean color satellites.

also varies annually. The most significant upwelling events occurred during the summers of 1994, 1996, and 2001, immediately following the most severe cooling seasons noted in Figure 3b. The summer of 1999 with the least amount of upwelling follows one of the mildest cooling seasons identified in Figure 3b. This prompts the hypothesis that the more severe cooling seasons may result in a colder and/or larger Cold Pool on the Middle Atlantic Bight continental shelf, and that this enlarged resource is then more readily available for the wind-driven forcing on the inner shelf side of the Cold Pool to produce more significant summer upwelling events.

[18] Annual variations in the duration and areal extent of the recurrent upwelling center offshore of the Mullica River Estuary was quantified (Figure 4) by its surface signature as observed in the satellite thermal imagery. For this plot, upwelling was defined as a surfacing of the seasonal thermocline that drives a surface temperature difference (compared to offshore) of more than 2°C between 1 June and 20 September. The number of events and the total duration are plotted in Figure 4a. Over the 9-year time period, three to eight summer upwelling events were observed each year, producing an annual average of just over five events per year. The total number of upwelling days per season range from 20 to 66. The resulting annual

average number of upwelling days experienced each summer is 37, exactly one third of the total days examined each year. During the largest upwelling years, 1993 and 1994, cooler upwelled waters were at the surface for over half of the summer. The average lifetime of the upwelling events over the entire record was almost exactly one week (Figure 4b). Five of the nine years examined had average durations within a day of the total average. Durations were slightly higher in 1997, and slightly lower in 2000 and 2001, with the largest outlier in average duration being the nearly 2-week event average experienced in 1994. The spatial area of the maximum extent of each upwelling event was positively correlated with upwelling lifetime, but the variability was much less (Figure 4c). The average upwelling cycle for this upwelling center impacted about 150 km^2 of the inner shelf. Except for 1994 and 2001, almost every year the average maximum area was within 20 km^2 of this value. In 2001, the short durations resulted in small areal coverage, and in 1994, the approximately double average duration resulted in three times the areal coverage.

[19] The actual occurrence of upwelling events during any given year was found to depend on the prevailing/prior wind, total precipitation, and overall storm frequency. One of the major factors determining the initiation and duration of the upwelling was how often the downwelling favorable

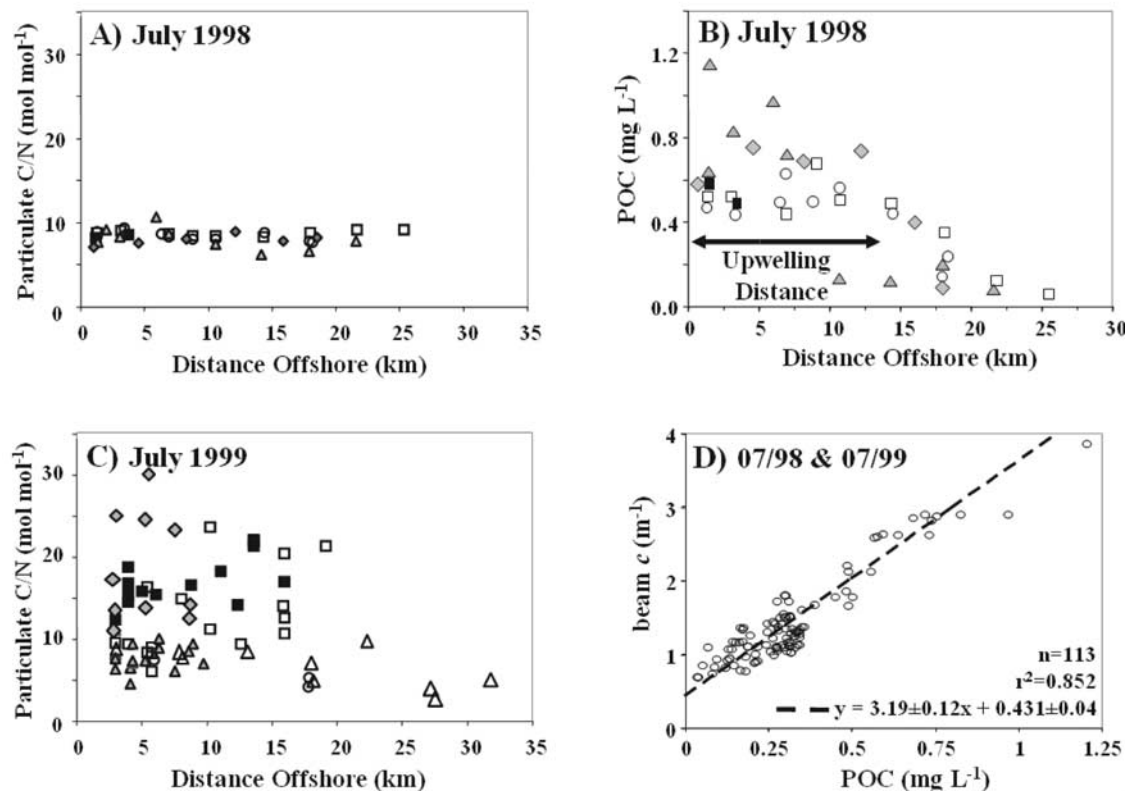


Figure 9. (a) The particulate carbon/nitrogen ratios taken during upwelling in summer 1998. (b) Particulate organic carbon concentrations were enhanced within the summer 1998 upwelling. (c) The carbon/nitrogen ratios collected in 1999 during periods of nonupwelling. The highly variable C/N values suggest a significant terrestrial influence. (d) The correlation between beam attenuation and POC for the POC data collected during the summers of 1998 and 1999.

winds were present. A good example is illustrated by comparing the summer 1994 and 1995 (Figure 5). The summer of 1994 had the largest upwelling event observed, while 1995 was one of the least active upwelling years despite both having similar protracted periods of upwelling favorable winds (Figures 5a and 5b). The big difference was that in 1995, a strong downwelling wind event pushed cold bottom water over 20 km farther offshore in mid-June (Figure 5d). In contrast in 1994, 10°C bottom water was almost always only 10 km offshore (e.g., Figure 5c) and thus only a small amount of upwelling favorable wind was required to initiate an event.

[20] Another factor important in determining the presence and absence of upwelling was precipitation. The spring and summer of 2000 was the wettest in a century for New Jersey [Kohut *et al.*, 2004], which increased the runoff from local rivers. The net result in summer 2000 was a jet of southward flowing low-salinity water during the upwelling season at LEO (Figure 6a) [Johnson *et al.*, 2003; Oliver *et al.*, 2004]. To the north of the LEO study site, cross-shore surveys clearly delineated the low-salinity water that was most likely from the Hudson River [Johnson *et al.*, 2003]. The Hudson waters had distinctly different optical characteristics than local coastal/estuarine waters because of enhanced phytoplankton, freshly produced CDOM and high detrital loads [Oliver *et al.*, 2004]. Local winds did

not heavily influence the behavior of the plume [Chant *et al.*, 2004], suggesting the forcing was dominated by the buoyancy-driven pressure gradient. Thus upwelling near the coast was retarded despite persistent southwesterly winds.

[21] The final feature influencing the lifetime of the coastal upwelling is storm frequency, which was highly variable year to year. For example, 1994 and 1998 had similar amounts of upwelling favorable wind, however the passage of frequent storms in 1998 (Figure 6b) disrupted the upwelling events by mixing the nearshore waters, thereby lowering the number of upwelling days during the summer.

3.2. Biogeochemical Impacts

[22] Shipboard sampling along a cross-shelf transect originating at the location of the LEO cabled observatory enables the composition of the material both within recurrent upwelling centers and just outside to be determined. Associated with a typical upwelling event is an immediate increase in water column turbidity sufficient to overwhelm the signals of any biological features present prior to the upwelling. Figure 7 from the cabled observatory is a well documented example. The lack of a phase lag between the increase in water column turbidity and the initiation of the upwelling indicated by the rapid decrease in temperature suggests that the source waters of the upwelling eddy

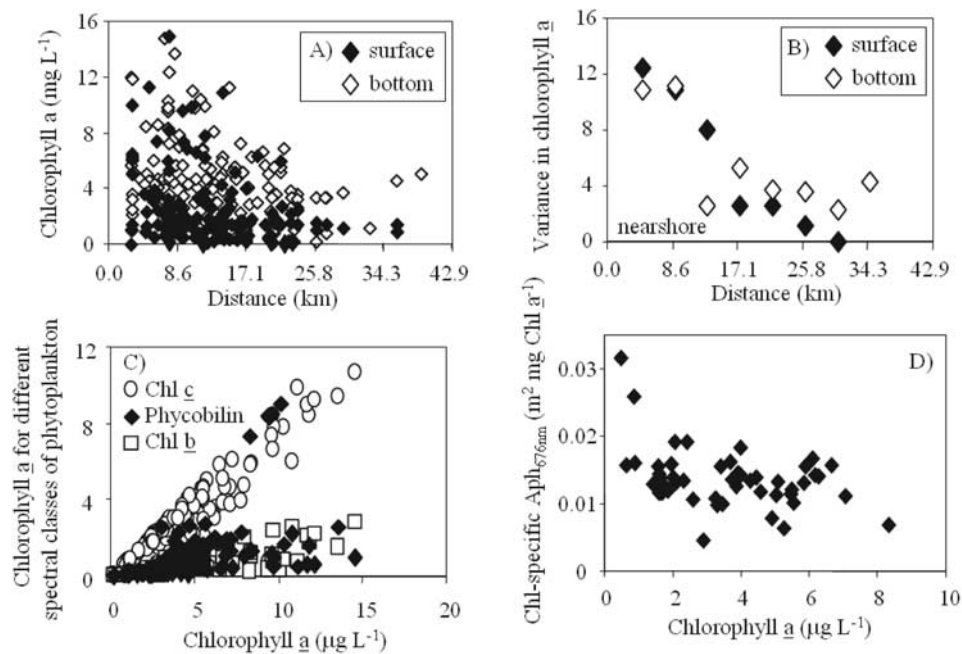


Figure 10. (a) The variability in chlorophyll *a* biomass as a function of longitude indicating that phytoplankton biomass in surface and bottom waters was greater nearshore. (b) The variance in the phytoplankton biomass was highest nearshore with the magnitude of the variance decreasing dramatically outside of the standard upwelling area. (c) The major spectral classes of phytoplankton present and their overall relation to total biomass is presented. Chlorophyll *c*-containing phytoplankton, primarily diatoms, dominated the phytoplankton biomass. While phycobilin-containing algae dominated offshore, the total chlorophyll levels were low. On some occasions phycobilin-containing algae, cryptophytes, were introduced from the local estuaries. Chlorophyll *b*-containing algae were never a major component within these waters. (d) The chl-specific absorption at 676 nm for filter pad measurements of phytoplankton were low (~ 0.01), consistent with the pigment package effect being large. The lowest values were found within the upwelling center.

already contained high organic carbon loads. Since this observation is typical, the total number of upwelling days provides a reasonable estimate of the amount of time that enhanced organic material is deposited within the upwelling eddy. This is in contrast to classical upwelling scenarios, such as Peruvian upwelling where a significant increase in phytoplankton concentration follows the upwelling initiation over a period of weeks as time is required for cells to reproduce.

[23] The source of the high-turbidity water associated with the onset of upwelling is revealed through cross-shelf shipboard surveys using towed ADCPs and undulating CTD/fluorometers. Recall that the surface flow field in the vicinity of the recurrent upwelling center consisted of a cyclonic eddy within the cold center, and a northward flowing surface jet on the warm side of the upwelling front that made a sharp anticyclonic turn around the cold center (Figure 2e). Subsurface current observations on the cross-shelf transects on the northern side of a typical upwelling center (Figure 8a) indicated a northward flowing upwelling jet confined to the upper water column above the thermocline on the offshore side, and a previously undetected southward flowing jet on the nearshore side. The nearshore jet is observed within the now spread isotherms of the offshore thermocline. The corresponding fluorometer sec-

tions (Figure 8b) indicated that the highest phytoplankton concentrations were located within or below the subsurface jet, leading to the hypothesis that the increase in phytoplankton and organic matter within the upwelling center was initially dominated by advective loading from the north. Whether the source of the material is from offshore and/or is resuspended from coastal benthic communities near the bottom is unresolved. This organic carbon rich southward flowing jet soon encounters the topographic high along the southern sampling line, and currents are observed to veer offshore (Figure 8c) as described in detail by *Chant et al.* [2004]. Organic material is distributed offshore into the upwelling center, spreading at the thermocline level (Figure 8d).

[24] The increases in the ocean turbidity during upwelling events reflects enhanced concentrations of inorganic/organic particulates and dissolved substances. To begin to determine the nature of the suspended particles, the particulate carbon/nitrogen ratios were calculated from water samples collected along a cross-shelf transect during an upwelling event and again under nonupwelling conditions. The C/N (mol mol^{-1}) ratio of suspended biogenic material during the upwelling event (8.3 ± 0.6) was remarkably constant (Figure 9a) and only slightly higher than marine plankton (the canonical 6.6 Redfield ratio). During non-

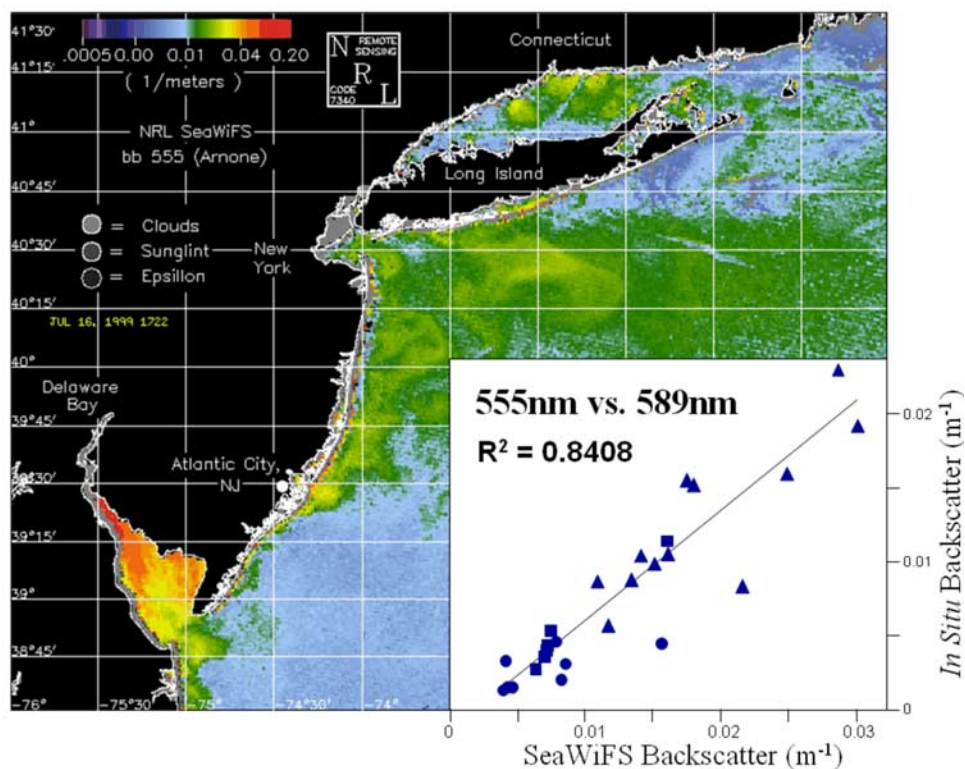


Figure 11. SeaWiFS-derived light backscatter at 555 nm for the New York Bight region in July 1999. The inset shows the comparison of in situ measured backscatter (measured using a HOBI Labs Hydrosatt-6 at LEO) with backscatter measurements derived from SeaWiFS. The different symbols indicate data collected at different days during the summer 1999 field effort. Note the linear scale on the inset.

upwelling periods, the C/N ratios were much higher, ranging from 10 to 30 (Figure 9c). This suggests that the dominant organic components within the more turbid eddy were phytoplankton.

[25] To determine the potential contribution of terrestrial and authigenic inorganic particles to total suspended particulate matter (SPM), the particulate Al and Fe concentrations were examined. The upwelling environment was largely organic in nature, and particulate Al and Fe concentrations decreased about seven fold and eighteen fold, respectively, with distance offshore. Particulate Al was $\sim 150 \text{ nmol kg}^{-1}$ inshore and dropped to $\sim 20 \text{ nmol kg}^{-1}$ at 22 km offshore. Fe displayed very high concentrations inshore ($\sim 360 \text{ nmol kg}^{-1}$) and fell off rapidly to $\sim 20 \text{ nmol kg}^{-1}$ at an offshore distance of 22 km. The Fe/Al ratios were highest inshore and decreased offshore to ratios similar to average crustal material [Wedepohl, 1995]. Our estimates yield a maximum inorganic particle concentration of $<8\%$ by mass (assuming Al is 8% of average crustal particles [Wedepohl, 1995] and that excess Fe (where $\text{Fe}_{\text{excess}} = \text{Fe}_{\text{total}} - (\text{Fe}/\text{Al})_{\text{crust}} \text{Al}_{\text{total}}$) was present as $\text{Fe}(\text{OH})_3$). Applying inorganic mass corrections to SPM did not significantly affect the slope or intercept of the regression equations between the in situ optical signals and organic carbon during upwelling events, suggesting robust organic carbon estimates might be derived from bio-optical maps.

[26] Similar to other studies [Peterson, 1977; Bishop, 1986; Gardner *et al.*, 1985], particulate organic carbon (POC) concentration was correlated to bio-optical variables regardless if the water was upwelled or not. The slope between SPM and water-corrected beam transmissometry ($c-c_w$) for inner shelf surface waters ($0.817 \pm 0.095 \text{ kg mg}^{-1} \text{ m}^{-1}$) was similar to values reported by Peterson [1977] for continental shelf waters off Oregon ($0.7 \pm 0.15 \text{ kg mg}^{-1} \text{ m}^{-1}$), by Bishop [1986] in productive northwest Atlantic slope waters $>100\text{-m}$ depth ($0.87 \pm 0.16 \text{ kg mg}^{-1} \text{ m}^{-1}$; 1986), and by Gardner *et al.* [1985] for northwest Atlantic continental rise nepheloid ($0.83 \pm 0.024 \text{ kg mg}^{-1} \text{ m}^{-1}$) and midwaters ($0.85 \pm 0.016 \text{ kg mg}^{-1} \text{ m}^{-1}$). Our intercept 0.086 ± 0.226 is not significantly different from zero after the attenuation of particle free water was subtracted from all data points.

[27] About 95% of the variance in POC can be explained by c alone indicating that robust estimates of POC can be made with the optical properties in these inner shelf surface waters during summer upwelling (Figure 9d). Our slope of $2.80 \pm 0.18 \text{ kg mg}^{-1} \text{ m}^{-1}$ between $c-c_w$ 660 and POC in inner shelf surface waters is significantly lower than values of 5.09 ± 0.758 and 3.62 ± 0.283 reported for northwest Atlantic slope surface waters [Bishop, 1986; Bishop *et al.*, 1992], and $5.28 \pm 0.35 \text{ kg mg}^{-1} \text{ m}^{-1}$ reported for surface waters of the equatorial Pacific [Bishop, 1999]. The corrected intercept of our regression ($0.28 \pm 0.12 \text{ m}^{-1}$)

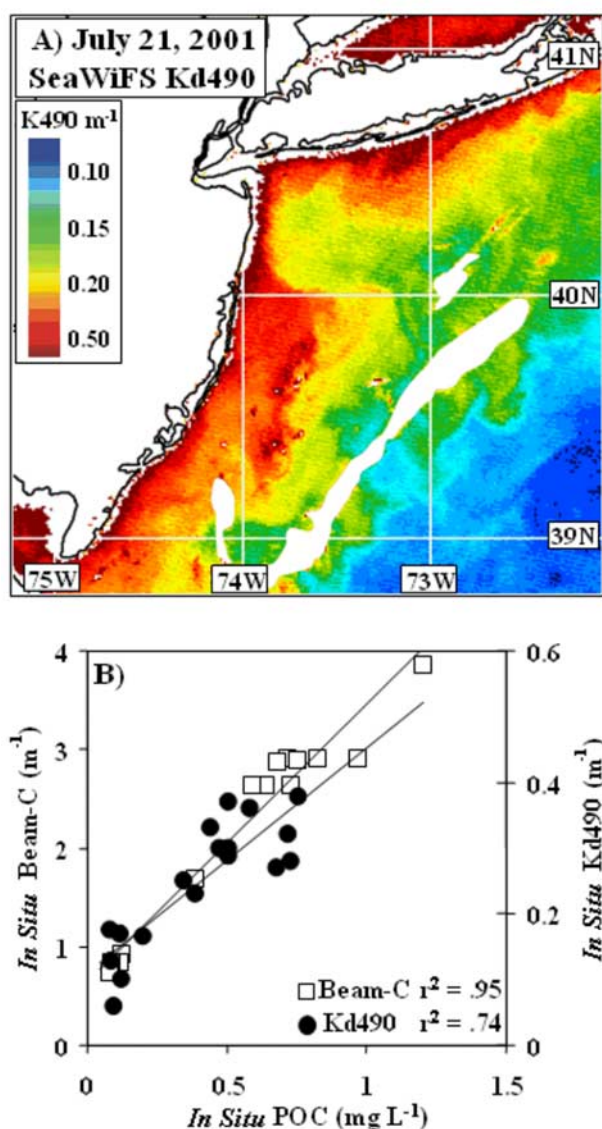


Figure 12. Using (a) satellite-derived diffuse attenuation and (b) POC regression determined from in situ data, the average POC load within the summer upwelling center was estimated. The data in Figure 12b were collected from in situ measurements at LEO during the summer of 1998.

is significantly greater than zero indicating the presence of dissolved organic material and the presence of some inorganic particles.

[28] An examination of the data indicated that the regression slopes relating $c-c_w$ to POC were depressed moving from offshore to inshore waters. The lower slopes of our regressions were potentially a shift to larger particle sizes in inshore locations, since slope was inversely related to particle size [Baker and Lavelle, 1984]. Productive inner shelf waters are high-energy environments with high-SPM loads dominated by larger particles comprising allochthonous inorganic and organic material, resuspended sediments, and large ($>5\text{-}\mu\text{m}$) phytoplankton [Chavez, 1989]. Oligotrophic waters are typically characterized by low SPM loads and small autotrophic cells ($<1\text{-}\mu\text{m}$) cells [Chavez, 1989;

Chisholm *et al.*, 1988; Chisholm, 1992]. The impact of cell size can be twofold. First, larger cells are more effective at scattering photons in the forward direction [Baker and Lavelle, 1984], which would in turn have a higher probability of being scattered into the acceptance angle of the light detector [Zanveld *et al.*, 1982]. Secondly, size impacts the efficiency of light attenuation of a particle. Spinrad [1986] demonstrated that the relative refractive index of the volume-specific particle beam attenuation coefficient is dependent on size distribution of the particles. Both of these effects will result in oligotrophic surface waters having higher c versus SPM or POC slopes than more productive inner shelf surface waters.

[29] Similar to POC, the chlorophyll a (Chl a) values were significantly higher nearshore with the highest concentrations ($>10\ \mu\text{g L}^{-1}$) associated with the upwelled waters (Figure 1b and Figure 10a). In addition to higher concentrations, the variance in the Chl a concentrations were also highest near the coast (Figures 10a and 10b). Phytoplankton within the upwelled waters were dominated by chromophytic algae with diatoms being the major phytoplankton taxa present (Figure 10c). Offshore waters were dominated largely by the phycobilin-containing picoplankton *Synechococcus*. An estuarine influence in the nearshore waters was often delineated by the presence of the phycobilin-containing cryptophytes (Figure 10c). The presence of cryptophytes was rare during upwelling and chlorophyll c algae dominated the phytoplankton communities. Chlorophytes were never a dominant taxa in these waters (Figure 10c). Within the upwelling waters the magnitude of Chl a -specific absorption was depressed in wavelengths of maximal absorption in the nearshore waters (Figure 10d), consistent with an increase in the pigment packaging effect [Morel and Bricaud, 1986]. This confirms that the upwelling was dominated by large phytoplankton that could account for the variability for correlation slopes between the POC and optical signals across different waters masses. This illustrates the difficulty in applying open ocean

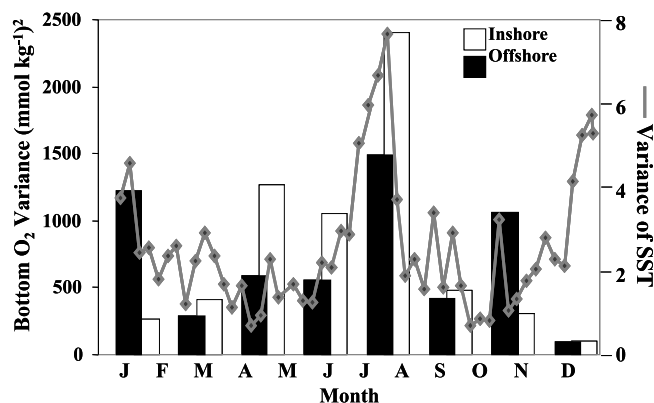


Figure 13. Bottom oxygen variance values computed in 1.5-month intervals for the data collected in the LEO research area from 1994 to 1997. Offshore (18–30 km) variances are more variable compared to inshore (5–15 km) variances, which peak during the summer upwelling season. Satellite SST were measured 6 km offshore from 1993 to 2001.

empirical relationships in coastal waters where empirical relationships need to be derived locally. Given this, a local regression was used, which worked in both upwelling and nonupwelling conditions thus allowing for reasonable estimates of POC to be derived optically.

[30] Recently approaches have been developed that estimate POC concentrations using satellite imagery [Stramski *et al.*, 1999]. These estimates are based on empirical correlations between POC and either the apparent or inherent optical properties, which can be estimated from remote sensing reflectance. This approach differs from traditional satellite algorithms that estimate parameters such as chlorophyll *a* by band ratioing of water leaving radiances at different wavelengths [cf. Bissett *et al.*, 2001]. This traditional approach is compromised in optically complex waters (most coastal systems) where the presence of optically active constituents other than phytoplankton (sediments, dissolved organics, etc.) impact the relative reflectance of light at different wavelengths, thereby compromising the band ratio approach. The wide optical gradients associated with the upwelling provided an ideal location to ground truth and validate these new satellite algorithms (Figure 11).

[31] Using calibrated satellite-derived optical properties (Figure 12a) and the in situ POC regressions (Figure 12b), we could estimate the average POC load associated with a typical summer upwelling event (Figure 12b). The recurrent upwelling centers typically contain around 1 mg POC L^{-1} (or $8.3 \times 10^4 \mu\text{mol POC m}^{-3}$) based on optical imagery collected since 1998. The upwelling leads to enhanced loads of phytoplankton that dominate the upper 8–10 m of the waters but are deposited in the lower 5 m of the water column via sinking marine snow and/or subduction. Marine snow and transparent exopolymers (TEP) concentrations are high in these waters during upwelling (J. Seebo, personal communication), promoting the efficient transfer of organic matter from the surface to the bottom waters. Consistent with this observation was that detrital loads were significant during the upwelling events accounting for up to 30% of the overall optical load present [Schofield *et al.*, 2004]. Assuming a respiratory quotient of $1.1 \text{ mol O}_2 \text{ mol}^{-1} \text{ }^\circ\text{C}$ [Falkowski and Raven, 1997], then microbial oxidation of the organic carbon transported to the bottom waters would potentially deplete $9.1 \times 10^4 \mu\text{mol O}_2 \text{ m}^{-3}$ (or $182 \mu\text{mol O}_2 \text{ kg}^{-1}$ given that material present in the upper 10 m is being deposited into the lower 5 m). Typical bottom oxygen levels in summer are close to $240 \mu\text{mol kg}^{-1}$. The potential respiratory demand could thus deplete 75% of the oxygen, making bottom waters borderline hypoxic at $58 \mu\text{mol O}_2 \text{ kg}^{-1}$. This simplified budget assumes that there is a strong thermal cap (as noted by Swanson and Parker [1988]) and that all carbon is consumed. Additionally, the presence of a turbid surface layer will decrease any potential productivity, and corresponding oxygen production, in the bottom layer, further exasperating the respiratory driven declines of oxygen in bottom waters. The magnitude of the depressed bottom and benthic productivity warrants further study. Finally, as the average POC estimate was based on satellite imagery and that phytoplankton concentrations were usually higher at depth below the detection depth of the satellites, the potential oxygen depletion could be much higher.

[32] Given that upwelling could potentially drive the coastal bottom water hypoxia, it would be expected that the variability in the bottom water oxygen levels and the SST should show some relationship to each other over time. Pooling SST measurements and several years of bottom water chemistry data [Boehme *et al.*, 1998], the variance in the SSTs and bottom water O_2 concentrations were both greatest in July during peak periods of upwelling (Figure 13). Furthermore, the variance in the oxygen saturation is greatest in nearshore waters (Figure 13), which are more often impacted by the upwelling. The offshore waters are only impacted by upwelling when the events are very long lived as in 1994 (Figure 4), which is rare.

4. Summary and Conclusion

[33] This paper summarizes research results related to coastal upwelling, the resulting phytoplankton blooms, and their potential effect on bottom dissolved oxygen concentrations on the New Jersey shelf. An alternative explanation presented here for the historically observed distribution of recurrent hypoxia is that the hypoxia regions are associated with topographically driven recurrent upwelling centers. The recurrent upwelling centers are established during southwesterly winds associated with the atmospheric Bermuda High. The center offshore of the Mullica River estuary typically is observed five times each summer, lasts for about a week each time, and covers an average area of about 150 km^2 . The most significant upwelling centers occur following severe cooling seasons. The actual occurrences of upwelling are further modulated by the proximity of the inshore side of the Cold Pool to shore, by the strength of the Hudson River plume, and by the occurrence of summer mixing storms. The upwelling centers consist of a northward flowing surface jet on the offshore side of the upwelling front, and a southward countercurrent located right at the coast, forming a cyclonic eddy within the upwelling center. Chant *et al.* [2004] found that the upwind jet transported sufficient cold water to fill a typical upwelling center during a typical week-long lifetime. This manuscript indicates that the increase in phytoplankton concentrations occurs immediately upon the onset of upwelling conditions, indicating that the phytoplankton signal is dominated by advection. The highest phytoplankton concentrations are observed within the upwind jet. The amount of phytoplankton concentrated by the jet within the upwelling center is sufficient to deplete oxygen levels to the typically observed hypoxic conditions if the required thermal cap is allowed to develop without the occurrence of a mixing storm. As usual, research on one scientific hypothesis often leads to the development of new research directions. The results of this study point to a need for long-term monitoring of the Cold Pool to determine its relation to climate variability, since its size and/or strength appear to be related to the strength and frequency of the coastal upwelling signals, and to spatial monitoring of the shelf phytoplankton distributions over seasonal scales, since the rapid increase in phytoplankton concentrations within the upwelling centers are dominated by the advection of phytoplankton populations from a wider shelf area.

[34] **Acknowledgments.** This decade-long effort that began with the deployment of a single S4 current meter in 1993 and concluded with the four summer Coastal Predictive Skill Experiments in 1998–2001 was sustained through the collaborative efforts of numerous researchers from academic institutions (APL, Cornell, Dalhousie, Lamont Doherty, Mote Marine Labs, OSU, Rutgers, Scripps, UCSB, U. Delaware, WHOI), federal and nonprofit research labs (FERI, NAVAIR, NOAA-NESDIS, NRL, and NUWC), and corporate partners (CODAR, Satlantic, SeaSpace, Sequoia Inc., HOBI Inc., and Webb Inc.). We thank an anonymous reviewer and Richard Jahnke for constructive reviews. Core funding was provided by ONR (N00014-97-0797, N0014-99-0196, and N00014-00-1-0724), NOPP (N00014-97-1-1019 and N00014-98-1-0815), NSF (OCE-9314823), NURP (NA-76RU0165), and the Great State of New Jersey.

References

- Atwood, D. K., T. E. Whitledge, J. H. Sharp, A. Y. Cantillo, G. A. Berberian, J. M. Parker, P. G. Hanson, J. P. Thomas, and J. E. O'Reilly (1979), Chemical factors, in *Oxygen Depletion and Associated Benthic Mortalities in New York Bight, 1976*, NOAA Prof. Pap. 11, edited by R. L. Swanson and C. J. Sindermann, pp. 79–123, Natl. Oceanic and Atmos. Admin., Silver Spring, Md.
- Austin, J. A., and S. J. Lentz (2002), The inner shelf response to wind-driven upwelling and downwelling, *J. Phys. Oceanogr.*, **32**, 2171–2193.
- Baker, E. T., and J. W. Lavelle (1984), The effect of particle size on the light attenuation coefficient of natural suspensions, *J. Geophys. Res.*, **89**, 8197–8203.
- Beardsley, R. C., and W. C. Boicourt (1981), On estuarine and continental-shelf circulation in the Middle Atlantic Bight, in *Evolution of Physical Oceanography*, edited by B. A. Warren and C. Wunsch, pp. 198–233, MIT Press, Cambridge, Mass.
- Bernstein, R. L. (1982), Sea surface temperature estimation using the NOAA-6 advanced very high resolution radiometer, *J. Geophys. Res.*, **87**, 9455–9465.
- Bishop, J. K. B. (1986), The correction and suspended particulate matter calibration of Sea Tech transmissometer data, *Deep Sea Res.*, **33**, 121–134.
- Bishop, J. K. B. (1999), Transmissometer measurement of POL, *Deep Sea Res.*, **Part I**, **46**, 353–369.
- Bishop, J. K. B., R. C. Smith, and K. Baker (1992), Springtime distributions and variability of biogenic particulate matter in Gulf Stream warm-core ring 82B and surrounding N. W. Atlantic waters, *Deep Sea Res.*, **Part A**, **39**, 295–326.
- Bissett, W. P., O. Schofield, S. M. Glenn, J. J. Cullen, W. K. Miller, A. J. Plueddemann, and C. D. Mobley (2001), Resolving the impacts and feedbacks of ocean optics on upper ocean ecology, *Oceanography*, **14**, 3–53.
- Boehme, S. E., C. L. Sabine, and C. E. Reimers (1998), CO₂ fluxes from a coastal transect: A time-series approach, *Mar. Chem.*, **63**, 49–67.
- Chant, R. J. (2001), Evolution of near-inertial waves during an upwelling event on the New Jersey inner shelf, *J. Phys. Oceanogr.*, **31**, 746–764.
- Chant, R. J., S. Glenn, and J. Kohut (2004), Flow reversals during upwelling conditions on the New Jersey inner shelf, *J. Geophys. Res.*, **109**, C12S03, doi:10.1029/2003JC001941.
- Chavez, F. P. (1989), Size distribution of phytoplankton in the central and eastern tropical Pacific, *Global Biogeochem. Cycles*, **3**, 27–35.
- Chisholm, S. W. (1992), Primary productivity and plankton size, *Biogeochemical Cycles in the Sea*, edited by P. G. Falkowski and A. D. Woodhead, pp. 213–237, Plenum, New York.
- Chisholm, S. W., R. J. Olson, E. R. Zettler, R. Goericke, J. B. Waterbury, and N. A. Welschmeyer (1988), A novel free-living prochlorophyte abundant in the oceanic euphotic zone, *Nature*, **334**, 340–343.
- Cleveland, J. S., and A. D. Weidemann (1993), Quantifying absorption by aquatic particles: A multiple scattering correction for glass-fiber filters, *Limnol. Oceanogr.*, **38**, 1321–1327.
- Cullen, J. T., M. P. Field, and R. Sherrell (2001), The determination of trace elements in filtered suspended marine particulate material by sector field HR-ICP-MS, *J. Anal. At. Spectrom.*, **16**, 1307–1312.
- Falkowski, P. G., and J. Raven (1997), *Aquatic Photosynthesis*, 375 pp., Blackwell, Malden, Mass.
- Falkowski, P. G., T. S. Hopkins, and J. J. Walsh (1980), An analysis of factors affecting oxygen depletion in the New York Bight, *J. Mar. Res.*, **38**, 479–506.
- Figley, W. B., Pyle, and B. Halgren (1979), Oxygen depletion and associated benthic mortalities in New York Bight, 1976, in *Socioeconomic Impacts*, edited by R. L. Swanson and C. J. Sindermann, pp. 315–322, Natl. Oceanic and Atmos. Admin., Silver Spring, Md.
- Friederich, G. E., L. A. Codispoti, and C. M. Sakamoto (1991), An easy-to-construct automated Winkler titration system, *MBARI Tech. Rep. 91-6*, Monterey Bay Aquarium Res. Inst., Moss Landing, Calif.
- Gardner, W. D., S. P. Chung, M. J. Richardson, and I. D. Walsh (1985), The oceanic mixed-layer pump, *Deep Sea Res.*, **42**, 757–775.
- Glenn, S. M., and M. F. Crowley (1997), Gulf Stream and ring feature analyses for forecast model validation, *J. Atmos. Oceanic Technol.*, **14**, 1366–1378.
- Glenn, S. M., M. F. Crowley, D. B. Haidvogel, and Y. T. Song (1996), Underwater observatory captures coastal upwelling off New Jersey, *Earth Space*, **9**, 9–11.
- Glenn, S. M., D. B. Haidvogel, O. Schofield, J. F. Grassle, C. J. von Alt, E. R. Levine, and D. C. Webb (1998), Coastal predictive skill experiments at the LEO-15 national littoral laboratory, *Sea Technol.*, **39**, 63–69.
- Grassle, J. F., S. M. Glenn, and C. von Alt (Eds.) (1998), *Ocean Observing Systems For Marine Habitats*, paper presented at Ocean Community Conference '98, Sea Technology.
- Hicks, D. C., and J. R. Miller (1980), Meteorological forcing and bottom water movement off the northern New Jersey coast, *Estuarine Coastal Shelf Sci.*, **2**, 63–571.
- Houghton, R. W., R. Schlitz, R. C. Beardsley, B. Butman, and J. L. Chamberlin (1982), The Middle Atlantic Bight cold pool: Evolution of the temperature structure during summer 1979, *J. Phys. Oceanogr.*, **12**, 1019–1029.
- Johnson, D. R., J. Miller, and O. Schofield (2003), Dynamics and optics of the Hudson River outflow plume, *J. Geophys. Res.*, **108**(C10), 3323, doi:10.1029/2002JC001485.
- Kishino, M., M. Takahashi, N. Okami, and S. Ichimura (1985), Estimation of the spectral absorption coefficients of phytoplankton in the sea, *Bull. Mar. Sci.*, **37**, 634–642.
- Kohut, J. T., and S. M. Glenn (2003), Improving HF radar surface current measurements with measured antenna beam patterns, *J. Atmos. Oceanic Technol.*, **20**, 1303–1316.
- Kohut, J. T., S. M. Glenn, and D. E. Barrick (1999), SeaSonde is integral to coastal flow model development, *Hydro Int.*, **3**, 32–35.
- Kohut, J. T., S. M. Glenn, and R. J. Chant (2004), Seasonal current variability on the New Jersey inner shelf, *J. Geophys. Res.*, **109**, C07S07, doi:10.1029/2003JC001963.
- McClain, E. P., W. G. Pichel, and C. C. Walton (1985), Comparative performance (AVHRR) based multichannel sea surface temperatures, *J. Geophys. Res.*, **90**, 11,587–11,601.
- Millie, D. F., G. L. Fahnenstiel, H. J. Carrick, S. E. Lohrenz, and O. Schofield (2001), Spatial variation in Lake Michigan phytoplankton composition during sediment resuspension events, *Verh. Int. Verein. Limnol.*, **28**, 1216–1220.
- Moores, C. N. K., J. Fernandez-Partagas, and J. F. Price (1976), Meteorological forcing fields of the New York Bight (first year's progress report), *Tech. Rep. TR76-8*, Rosenstiel School of Mar. and Atmos. Sci., Univ. of Miami, Miami, Fla.
- Morel, A., and A. Bricaud (1986), Inherent optical properties of algal cells including picoplankton: Theoretical and experimental results, in *Photosynthetic Picoplankton*, edited by T. Platt and W. K. W. Li, *Can. Bull. Fish. Aquat. Sci.*, **214**, 521–559.
- Oliver, M. J., O. Schofield, T. Bergmann, S. Glenn, C. Orrico, and M. Moline (2004), Deriving in situ phytoplankton absorption for bio-optical productivity models in turbid waters, *J. Geophys. Res.*, **109**, C07S11, doi:10.1029/2002JC001627.
- Peterson, R. E. (1977), A study of suspended particulate matter: Arctic Ocean and Northern Oregon Continental Shelf, Ph.D. thesis, Oregon State Univ., Corvallis.
- Saunders, P. M. (1977), Wind stress on the ocean over the eastern continental shelf of North America, *J. Phys. Oceanogr.*, **7**, 555–566.
- Schofield, O., T. Bergmann, W. P. Bissett, F. Grassle, D. Haidvogel, J. Kohut, M. Moline, and S. Glenn (2002), Linking regional coastal observatories to provide the foundation for a national ocean observation network, *IEEE J. Oceanic Eng.*, **27**, 146–154.
- Schofield, O., W. P. Bissett, T. K. Frazer, D. Iglesias-Rodriguez, M. A. Moline, and S. Glenn (2003), Development of regional coastal ocean observatories and the potential benefits to marine sanctuaries, *Mar. Technol. Soc. J.*, **37**, 54–67.
- Schofield, O., T. Bergmann, M. J. Oliver, A. Irwin, G. Kirkpatrick, P. W. Bissett, M. A. Moline, and C. Orrico (2004), Inversion of spectral absorption in the optically complex coastal waters of the Mid-Atlantic Bight, *J. Geophys. Res.*, doi:10.1029/2003JC002071, in press.
- Song, Y. H., A. Marx, J. Muller, G. Woehlke, M. Schliwa, A. Krebs, A. Hoenger, and E. Mandelkow (2001), Structure of a fast kinesin: Implications for ATPase mechanism and interactions with microtubules, *EMBO J.*, **20**, 6213–6225.
- Spinrad, R. W. (1986), A calibration diagram of specific beam attenuation, *J. Geophys. Res.*, **91**, 7761–7764.

- Steimle, F. (1978), Dissolved oxygen levels in York Bight waters during 1977, *NOAA Tech. Memo. NMFS-NE 20*, N. E. Fish. Cent., Woods Hole, Mass.
- Stoddard, A., J. E. O'Reilly, T. E. Whittedge, T. C. Malone, and J. F. Malone (1986), The application and development of a compatible historical data based for the analysis of water quality management issues in the New York Bight, *IEEE Oceans*, 18, 1030–1035.
- Stramski, D., R. A. Reynolds, M. Kahru, and B. G. Mitchell (1999), Estimation of particulate organic carbon in the ocean from satellite remote sensing, *Science*, 285, 239–242.
- Swanson, R. L., and C. A. Parker (1988), Physical environmental factors contributing to recurring hypoxia in the New York Bight, *Trans. Am. Fish. Soc.*, 117, 37–47.
- Warsh, C. (1987), NOAA's Northeast Monitoring Program (NEMP): A report on progress of the first five years (1979–84) and a plan for the future, *NOAA Tech. Memo. NMFS-F/NEC-44*, pp. 9–20, N. E. Fish. Cent., Woods Hole, Mass.
- Wedepohl, K. H. (1995), The composition of the continental crust, *Geochim. Cosmochim. Acta*, 59, 1217–1232.
- Wright, S. W., S. W. Jeffrey, R. F. C. Mantoura, C. A. Llewellyn, T. Bjornland, D. Repeta, and N. Welschmeyer (1991), Improved HPLC method for the analysis of chlorophylls and carotenoids from marine phytoplankton, *Mar. Ecol. Prog. Ser.*, 77, 183–196.
- R. Arnone and A. Weidemann, Ocean Color Section, Naval Research Laboratory, Stennis Space Center, MS 39529, USA.
- T. Bergmann, R. Chant, M. Crowley, S. Glenn, D. Haidvogel, J. Kohut, M. Oliver, O. Schofield, and R. Sherrell, Coastal Ocean Observation Lab, Institute of Marine and Coastal Sciences, Rutgers University, New Brunswick, NJ 08901, USA. (oscar@imcs.marine.rutgers.edu)
- W. P. Bissett, Florida Environmental Research Institute, 4807 Bayshore Blvd. Suite 101, Tampa, FL 33611, USA.
- J. Cullen, School of Earth and Ocean Sciences, University of Victoria, P.O. Box 3055, STN CSC, Victoria, British Columbia, Canada V8W 3P6.
- J. Gryzmski, Division of Earth and Ecosystems Science, Desert Research Institute, 2215 Raggio Parkway, Reno, NV 89512, USA.
- M. A. Moline and C. Orrico, Biological Sciences Department, California Polytechnic State University, San Luis Obispo, CA 93407, USA.
- T. Song, Jet Propulsion Laboratory, California Institute of Technology, 4800 Oak Grove, MS 300-323, Pasadena, CA 91109-8099, USA.